Indian Journal of Pure & Applied Physics
Vol. 63, August 2025, pp. 698-706
DOI: 10.56042/ijpap.v63i8.18625

Modified Surface and Tuned Optical Band Gap of Polymer Nanocomposite Thin Films

Gurpreet Kaur Bhullar[a], Gagandeep[b], Seema Maheshwari[c], Rishi Kumar[d] & Ramneek Kaur[a*]

[a]P.G. Department of Physics, Mata Gujri College, Fatehgarh Sahib 140 406, India

[b]Chitkara University, Chandigarh-Patiala National Highway, Punjab 140 406, India

[c]P.G. Department of Chemistry, Mata Gujri College, Fatehgarh Sahib 140 406, India

[d] Department of Physics, Guru Nanak College Budhlada Punjab 151 502, India

Received: 7 April 2025; accepted: 11 June 2025

Thin films of nanocomposites, polyvinyl alcohol (PVA) dispersed with Zinc Oxide (ZnO) nanoparticles (nps) were deposited by solution casting method. Films were characterized for structural, optical, photoluminescent properties and topographical parameters. X-ray diffraction analysis confirmed the presence of ZnO, with improved crystallinity observed at higher ZnO concentrations. Ultraviolet-visible spectrum showed absorption at 289.00 nm for pure PVA and the addition of ZnO nanoparticles at 1 wt% and 5 wt% in the PVA matrix showed a shift in absorption peaks to 370.00 nm and 379.00 nm respectively. Photoluminescence spectroscopy showed strong emission peaks at 371 nm corresponding to near-band-edge. Atomic Force Microscopy ensured uniform dispersion of nanoparticles in the PVA matrix.

Keywords: Polyvinyl alcohol, Nanoparticles, Ultraviolet-Visible Spectroscopy, Photoluminescence Spectroscopy, Atomic Force Microscopy

1 Introduction

Polymer-based nanocomposites have garnered significant interest in recent years due to their improved mechanical, thermal, and optical properties compared to conventional polymers. These advanced materials find applications in various fields, including electronics, packaging, and biomedical engineering[1-4]. The main reason for improved properties is the combination of organic (polymer) and inorganic (nanoparticles) phases. The compatibility between the two phases alters the behavior of composite thin films. Polymer nanocomposites possess improved morphology which is dependent upon interactions between polymer and nanoparticles (nps). Optoelectronics properties of such films have shown high importance[5].

Among the different polymers, polyvinyl alcohol (PVA) stands out becausesome devices consisting of PVA are biocompatible[6,7]. PVA also has water solubility, excellent film-forming capabilities, and high thermal stability, it contains long molecular chains and hydroxyl groups due to which it has molecular interaction with nps[8-10]. The incorporation of metal oxide nps, such as zinc oxide (ZnO), into polymer matrices has been shown to further improve the functional properties of the resulting nanocomposite films.

ZnOnps are known for their unique optical, electronic, antimicrobial, and photocatalytic properties[11-14]. When dispersed in a PVA matrix, these nps can enhance mechanical strength and UV-blocking capability[15] ZnOnps also have high thermal stability due to which ZnO has emerged as a suitable nanoparticle for dispersion in polymer for preparing thin films.

The solution casting method is a widely used technique for preparing polymer/ZnO nanocomposite films, allowing for uniform dispersion and consistent composition of nps within the polymer matrix. It is a relatively simple and cost-effective method. This method ensures even distribution and avoids agglomeration, which can occur in other methods. Overall, the solution casting method proves to be an effective technique for preparing PVA/ZnO nanocomposite films with uniform thickness and desirable properties for advanced material applications with improved mechanical strength. Solution casting is a versatile and widely used technique for fabricating nanocomposite thin films. By selecting suitable polymers and nanoparticles with

*Corresponding author: E-mail: dhaliwalramneek@gmail.com

compatible chemical and physical properties, similar modifications in surface morphology and optical properties can be achieved across various systems. However, challenges such as ensuring uniform nanoparticle dispersion and preventing aggregation may arise, requiring careful optimization of processing conditions and surface functionalization for different materials.

Many researchers have developed ZnO-dispersed PVA thin films by using a variety of techniques such as polymeric nanocomposite explored membranes with elevated permittivity using PVA combined with ZnOnps for potential applications in flexible electronics[16], investigated how film thickness influences the electrical and optical properties of PVA/ZnO nanocomposite films to enhance their performance[17], PVA/ZnO films were used for degradation of organic dyes [18], nanocomposite films were also designed for gas sensors, PVA-InAℓO (organic-inorganic) oxide films were produced by dip coating[19]. The incorporation of ZnO nanoparticles into PVA matrices significantly enhances structural, optical, antibacterial, thermal, and dielectric properties. Compared to PVC/ZnO composites, which offer higher rigidity but lower flexibility[20], compared to other polymer-nanoparticle composites, PVA/ZnO nanocomposites demonstrate superior optical and structural properties, making them highly suitable for optoelectronic and UV-sensitive applications. Structurally, ZnO nanoparticles exhibit strong interaction with the hydroxyl groups of the PVA matrix, resulting in improved crystallinity, better nanoparticle dispersion, and reduced aggregation challenges commonly observed in composites with TiO_2, Fe_3O_4, or CdS nanoparticles. The uniform distribution of ZnO also contributes to a smoother surface morphology and enhanced film stability. Optically, ZnO's direct wide band gap and high exciton binding energy offer more efficient modulation of optical absorption and enhanced photoluminescence compared to fillers like CdS or TiO_2, which often suffer from lower emission stability and limited tunability. Moreover, ZnO is an environmentally benign and non-toxic material, giving PVA/ZnO composites an additional edge over Cd-based systems. These advantages collectively position PVA/ZnO nanocomposites as a more effective choice for applications requiring high optical responsiveness and structural robustness[21-28].

This research introduces a novel approach of fabricating polyvinyl alcohol (PVA) and zinc oxide (ZnO) nanoparticle-based nanocomposite thin films, focusing on the modification of their structural and optical properties. By incorporating ZnO nanoparticles into the PVA matrix, the study demonstrates the ability to tune the material's optical band gap and enhance its crystallinity. The work also highlights the uniform dispersion of ZnO nanoparticles within the polymer, which is crucial for achieving consistent material properties. This approach offers new opportunities for designing advanced materials with tailored optical characteristics, suitable for various optoelectronic applications, such as sensors, light-emitting devices, and solar cells[29,30]. The combination of these elements—structural, optical, and photoluminescent characteristics—demonstrates the potential of ZnO nanoparticle-dispersed PVA thin films for advanced material design and their role in enhancing the functionality of polymer nanocomposites. The nanocomposite thin films of ZnO nanoparticles dispersed in PVA were deposited by the solution casting method. These films were analyzed using X-ray diffraction (XRD), UV-visible, and photoluminescence (PL) emission spectroscopies and films were also scanned by using atomic force microscopy (AFM). By systematically studying the effects of nanoparticle concentration and distribution, we aim to provide insights into the design of polymer nanocomposite thin films with tailored properties.

2 Materials Used and Experimental Techniques

2.1 Materials and Substrates Used

Polyvinyl alcohol (PVA) [$(-C_2H_4O)_n$] was purchased from LobaChemie with the degree of polymerization ranging from 1700-1800, molecular weight of monomer (CH_2-CHOH) unit forming PVA is 67.64 g per mol.

Figure 1 shows the molecular structure of PVA (ACD Chem. Draw software). Zinc oxide (ZnO) nanopowder (<50 nm, purity 97%) from Sigma–Aldrich with molecular weight 81.39 g per mol. Chloroform (99% pure for high-performance liquid chromatography) used as a solvent for preparing nanocomposites, was purchased from LobaChemie. Acetone, sulfuric acid, methanol, hydrogen peroxide and dilute (2%) hydrofluoric acid obtained from SD fine chemicals were used for cleaning substrates. Ethanol (AR grade) was purchased from Merck.Glass

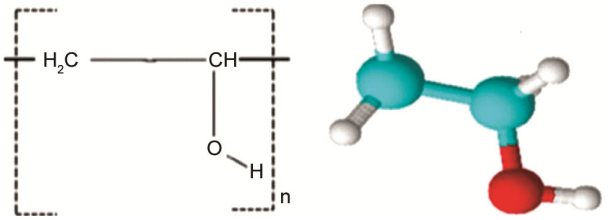

Fig. 1 — shows repeating monomer unit of polyvinyl alcohol and a three-dimensional view of monomer unit forming Polyvinyl alcohol (PVA). (Atoms are represented as red: Oxygen, white: Hydrogen, and blue: Carbon)

(15×15×1.2) mm, Quartz (15×15×1) mm and Silicon (15×15× 0.1) mm substrates were used to deposit film[31]. The surface area covered with thin film was same for each substrate. Glass substrate was rinsed with distilled water and acetone. The substrate was dried with a lint-free wipe. The quartz substrate was cleaned thoroughly by placing it in piranha solution (a mixture of sulfuric acid and hydrogen peroxide) in a beaker with ultrasonication for about 15 min, and finally, the substrate was rinsed with deionized water. The silicon substrate was immersed in warm acetone in a covered petri dish for approximately 10 min. After that, the substrate was transferred to methanol for around 3 minutes and then rinsed with deionized water.

2.2 Nanocomposite Materials and Thin film Fabrication by Solution Casting Method and characterization Techniques

1wt% and 5wt% nanocomposites were prepared by proper dispersion of polymer and ZnO nanoparticles in chloroform. A concentration of 1wt% represents the minimum threshold for XRD detection, while concentrations above 5 wt% may increase the risk of nanoparticle agglomeration.

In the case of 1 wt% composite: 0.1mg of ZnOnps and 9.9 mg of PVA were weighted on analytical electronic balance (Wensar, DAB 220) in a glass vial. For a 5 wt% composite system 0.5 mg of ZnOnps and 9.5 mg of PVA were put in another glass vial[32,33]. 5 ml of chloroform was added to both glass vials (containing 10 mg of total composite materials). 2 mg per ml concentrated dispersed solutions were obtained for both composites. Both glass vials were properly sealed with tight-fitting caps, and many layers of parafilm were made over caps to prevent evaporation of chloroform. Glass vials were mounted for ultrasonication (EQUIRON digital ultrasonic, rpm 180, 170 watts and 230VAC, 50 Hz) Solution were allowed to sonicate for 30 mins to get well-dispersed solutions.

Thin films were deposited by using the solution casting in a neat and clean environment, apparatus was placed in a case made up of glass and aluminium with a window opening on one side. Pre-cleaned and dried substrates were placed on the hot plate at nearly 60° C and the composite solution was spread dropwise in a uniform manner with the help of a syringe on the entire surface of the substrate. This temperature (~60 °C) ensured uniform solvent evaporation, enhanced crystallinity, and reduced defects. The temperature is also safely below the degradation point of PVA, preserving the polymer's structural integrity during film casting.

1 ml of each nanocomposite solution was put dropwise on the substrates (glass and quartz) separately, and proper drying time (a few seconds) was given to each drop. 0.5 ml solution was spread on a silicon wafer, to do atomic force microscopy. The solvent evaporated due to the temperature provided on the hot plate[34]. High temperatures lead to improved crystallinity and reduced defects in the structure of film. After the evaporation of the solvent thin film of nanocomposite material was deposited on the substrate. To prevent the contamination of films from surroundings, films were stored in an evacuated desiccator. The advantage of the solution casting method is that it doesn't require a special apparatus to experiment[35].Composite films deposited on glass substrates were analyzed using X-ray diffractometer analysis (XRD) spectroscopy with Cu–Kα (λ = 1.541 Å) radiation from a Philips XPERT–PRO MPD system, with an angle range 2θ from 10° to 80° at a generation tension of 45 kV and generator current of 40 mA. Glass substrate is amorphous due to which substrate peak was not obtained in the XRD spectrum.

Pure PVA and nanocomposite films deposited on pre-cleaned quartz substrate[36] were scanned by using Ultraviolet-visible (UV-Vis) spectroscopy (Shimadzu UV-1800 UV/Visible Scanning Spectrophotometer; 115 VAC). The absorption spectra were recorded in the wavelength range 200 nm to 800 nm. To analyze the effect of dispersion of nps on the band gap of nanocomposite films Tauc's plot was calculated from spectra.

Emission spectra for both the nanocomposite films and the pure PVA film were recorded using a Perkin Elmer photoluminescence (PL) system. The PL emission spectrum was recorded in the range 250 nm to 600 nm at excitation wavelength 270 nm.

A highly smooth Si wafer (roughness < 1nm)[37] was used to deposit the nanocomposite films to view the exact topography of the deposited film. It was done by using atomic force microscopy (NT-MDT), and Solver NEXT; Zelenograd, Moscow, Russia at a scanning rate of 1 Hz. The nanocomposite film surfaces were scanned (500 × 500 nm^2) with a silicon nitride (SiN) tip, which had a curvature radius of 2 nm, mounted on a cantilever with a resonance frequency of 87–230 kHz and a typical force constant of 5.1 nN per m. As polymers are soft materials, a non-contact mode of imaging was used to avoid film damage. Information including two-dimensional and three-dimensional views, grain analysis, average height profiles and histogram (size vs counts) from the images, was obtained by using NOVA P9 (Image Analysis 2.1.0.800) software.

3 Results and Discussion

XRD spectra of 1 wt% and 5 wt% ZnOnps in PVA nanocomposite films (Figure 2) showed intense peaks corresponding to ZnOnps at 31.81° (100), 34.44° (002), 36.25° (101), 47.76° (102), 56.92° (110), 63.44° (103) and 68.41° (112) at their corresponding planes, according to the JCPDS card number 36-1451. Broader peaks in both film spectra at 2θ = 20° were due to the slight orientation produced in the PVA molecule with the dispersion of nps[38-40]. The most intense peak in both cases is at 2θ =31.81°, with full width at half maximum (FWHM) of 0.296 for 5 wt% nanocomposite system and 0.299 for 1 wt% composite system. Particle size was calculated by using Scherer's Eq 1:

$$\tau = \frac{K\lambda}{\beta Cos\theta} \quad \ldots (1)$$

τ represents the particle size, and K is a shape factor that is dimensionless, typically close to one. The term λ denotes the wavelength of the X-rays, β refers to the broadening of the peak at half its maximum intensity, and θ indicates the Bragg angle at which strong peaks appeared. The calculated average particle size of PVA–ZnO (1wt%) nanocomposite was found to be 28.87 nm and in case of PVA–ZnO (5 wt%) it was 29.16 nm. It can be seen that the presence of nps can induce local ordering of polymer chains, promoting alignment. This ordering can result in improved mechanical strength and optical matrix from 1 wt % to 5 wt%, which resulted in an increased degree of crystallinity, properties. It can be seen that the dispersion weight of nps was increased in the

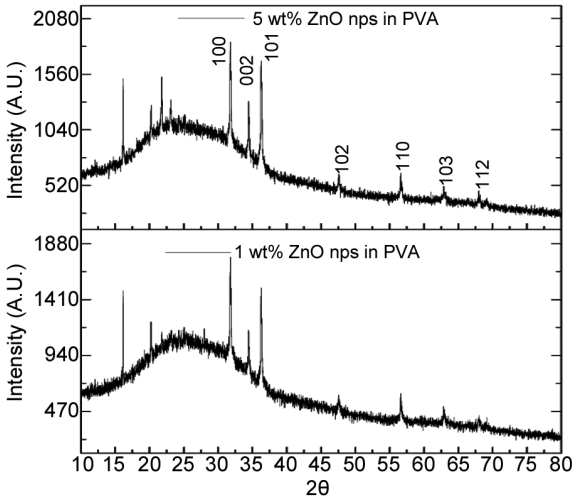

Fig. 2 — XRD spectra of 1 wt% and 5 wt% ZnO nanoparticles in PVA matrix, thin films, deposited on a glass substrate

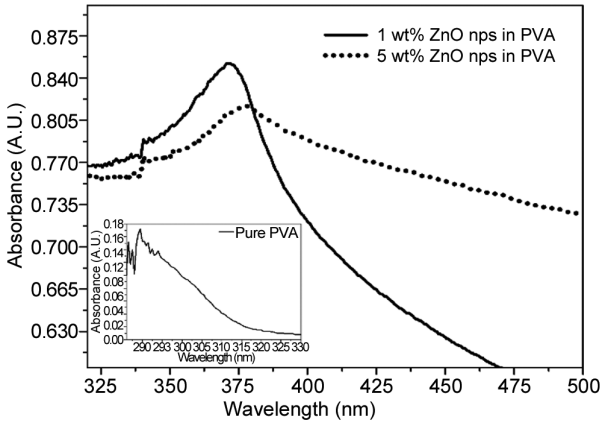

Fig. 3 — UV-Visible absorbance spectra of composite films of (1 and 5) wt% ZnOnps in PVA matrix deposited on a quartz substrate. The Inset of Fig.3 shows the absorbance spectra of pure PVA thin film

PVA corresponding to more content of ZnO in 5 wt% nanocomposite films[41].

Figure 3 shows absorption UV-Vis spectra for thin films of 1 wt% and 5 wt% ZnOnps in the PVA matrix. The spectrum for pure PVA thin film is shown in the inset of Fig. 3, absorbance peak was obtained at 289 nm. In 1 wt% nanocomposite thin film, the absorbance peak was obtained at 370 nm while in the case of the 5 wt% nanocomposite thin film, the spectrum showed an absorbance peak at 379 nm. The variation in the absorbance peak was attributed to the presence of ZnOnps, indicating an interaction between PVA and ZnO. Redshift (movement of the absorption peak in the direction of higher wavelength) was obtained with an increase in the concentration of ZnOnps in the PVA matrix.The optical (energy) band

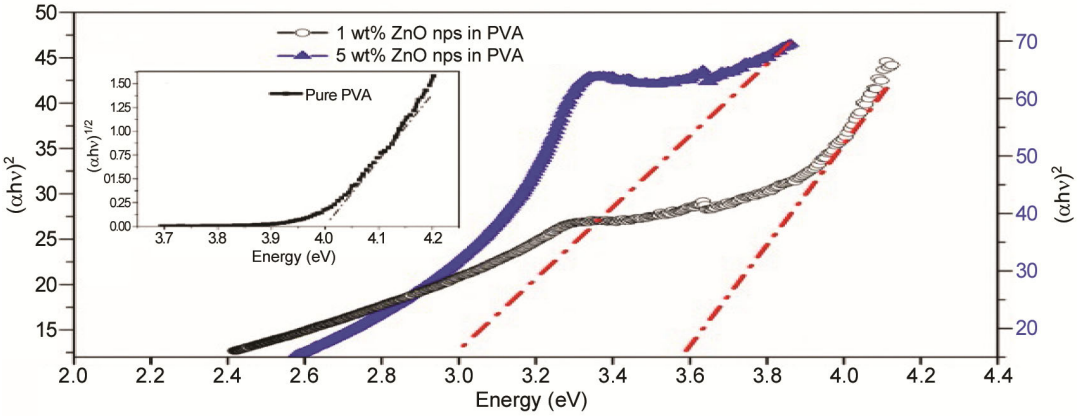

Fig. 4 — Shows Band energy curves forthin films of1 wt% and 5 wt% ZnOnps in PVA. The inset figure shows the band energy curve for pure PVA thin film

gap is determined from the UV-Vis spectra by constructing a Tauc's plot[42,43]. This method involves translating the spectra into a graphical representation where the absorption coefficient, which varies with frequency, is used according to Eq 2:

$$(\alpha h\nu)^{1/n} = A\,(E_g) \quad \ldots (2)$$

Here, A represents a parameter related to the interband transition probability, $E_g$is the optical band gap, and alpha(α) denotes the absorption coefficient. hν is the energy of the incident light, and n characterizes the nature of the transition: n=2 indicates a direct transition, while n=1/2 suggests an indirect transition[44-46]. The inset of Fig. 4 shows a plot of Energy (eV) versus $(\alpha h\nu)^{1/2}$, which reveals the direct transition for the pure PVA film. Extrapolating the straight line on this graph to the x-axis yields a direct band gap of 4.0 eV. Figure 4 illustrates an indirect band gap plot (Energy (eV) versus $(\alpha h\nu)^2$ for the composite films, highlighting the effects of both PVA and ZnO in the nanocomposites.

For the composite film with 1 wt% ZnOnps in PVA, the band gap is 3.6 eV, while for the 5 wt% ZnO nanocomposite film, the band gap shifts to 3.0 eV. It was due to the dependence of bandgap upon the concentration of ZnOnps, at higher concentrations, the quantum size effect becomes significant. The red shift in UV absorption from 289 nm to 370 nm (1wt%) and 379 nm (5 wt%) upon ZnO addition is due to strong interaction between ZnO nanoparticles and the PVA chains, leading to the formation of interfacial localized states, As a result, the π→π* or n→π* electronic transitions in the polymer matrix are affected, shifting the absorption to longer wavelengths resulting in reduction of optical band gap.

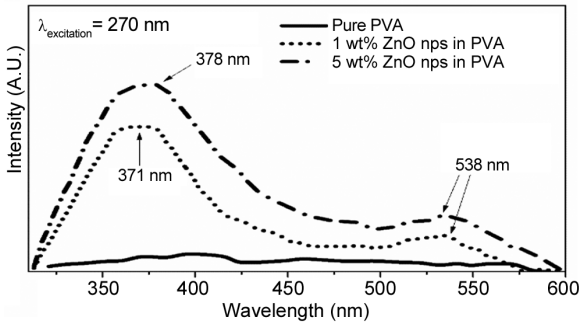

Fig. 5 — PL emission spectra at excitation wavelength 270 nm for pure PVA film, thin films of 1 wt% and 5 wt% of ZnOnps in PVA matrix

The conductivity of the composite may increase due to enhanced electron mobility, which can be understood at 5 wt% of ZnOnps, their interactions with PVA can modify the electronic structure, causing hybridization of electronic states and thus influencing the overall band gap. This tuning of the band gap can lead to applications in organic solar cells [47]. Moreover, ZnOnps in host matrix PVA will provide mechanical flexibility to organic solar cells, but the concentration of nanoparticles needs to be below the limit to avoid excessive brittleness or phase separation. Similar studies are reported by S.A. Khan *et al.*[48] deposited PVA/ZnO nanocomposite films (14.25%, ZnO) and 85.75% (PVA matrix)), showed that the optical direct bandgap decreased as ZnO concentration was increased in the polymer matrix. Reduction in band gap is reported at less wt% in our findings retaining the stability of the film. PL emission spectra at excitation wavelength 270 nm for pure PVA film, a thin film of 1 wt% and 5 wt% of ZnOnps in the PVA matrix are shown in Fig. 5. No emission peak is shown for a thin film of pure PVA. In composite

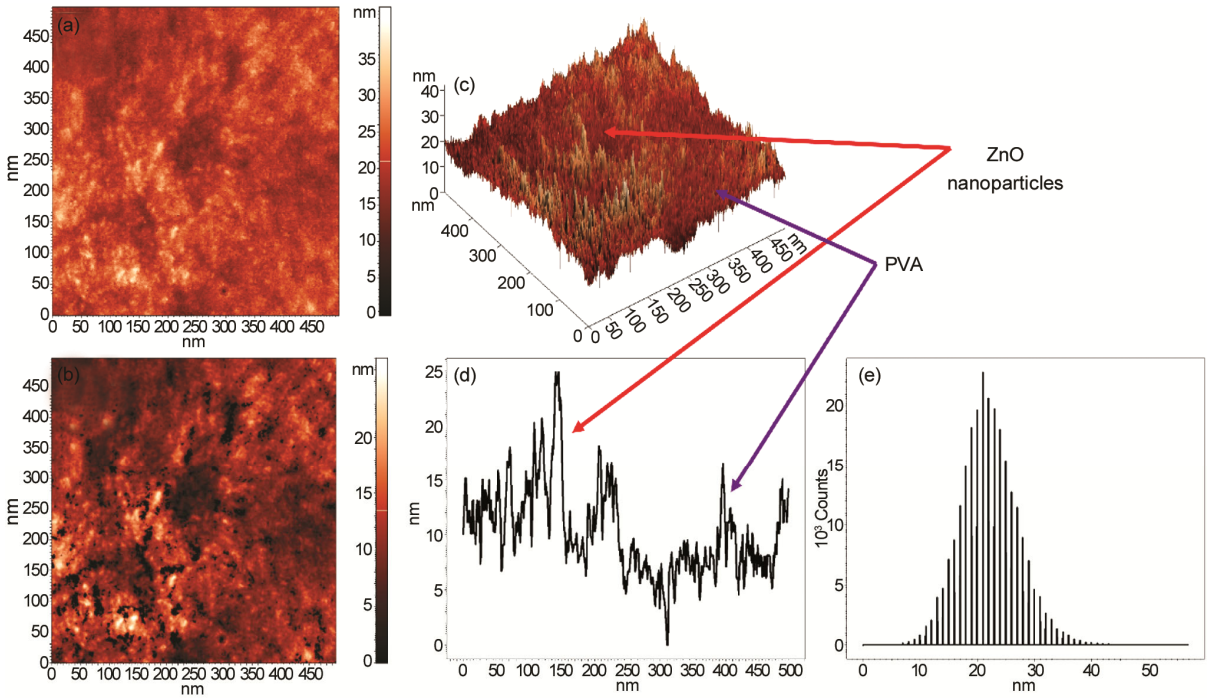

Fig. 6 — (a-e) shows the two-dimensional topographical map, grain size analysis, three-dimensional view, the average height profile and a histogram for particle size vs count receptively for a thin film of 1 wt% ZnOnps in PVA matrix deposited on a Si substrate

films containing ZnOnps embedded in a polymer matrix, two distinct emission peaks are observed. Using an excitation wavelength of 270 nm, the photoluminescence spectra exhibit an emission peak at 371 nm for 1 wt % ZnO and a slightly redshifted peak at 378 nm for 5 wt % ZnO. This shift and the near-band-edge (NBE) emission are significant for studying the optoelectronic quality and defect concentrations of ZnO in polymer matrices.

The emission peak at 371 nm for 1 wt% ZnO corresponds to the recombination of free excitons. These excitons, or electron-hole pairs, are bound by Coulombic forces within the ZnO crystal lattice. This near-band-edge (NBE) emission is characteristic of high-quality ZnO crystals with minimal defect levels, which contributes to a sharper and stronger photoluminescent signal. Jangir*et al*. reported similar PL features in studies of ZnO nanoparticles in polymer matrices, where low defect concentration maintained the excitonic emission[49] At a higher ZnO concentration of 5 wt%, the PL peak shifts slightly to 378 nm. This redshift may be attributed to increased interactions between ZnO particles. Higher ZnO loading can introduce strain in the crystal structure or create minor defect states, resulting in a slight reduction in the recombination energy and thus a redshifted emission. Similar red shifts with increasing ZnO Concentration have been reported aligning with observed PL characteristics in studies of ZnO - Polymer composite reported by Ristic *et al*.[50]

The near-band-edge emission is a critical feature for optoelectronic applications as it confirms the high optical quality of the ZnO crystals within the composite. This study's results, demonstrating NBE emission with minimal redshift, highlight the potential of PVA-ZnO composites in optoelectronics, where achieving defect-free excitonic recombination is essential. The second emission peak is obtained at 538 nm (green emission) for both thin films. Green emission is due to ZnO nps typically it occurs due to oxygen vacancies and zinc interstitials. Pure ZnO can exhibit visible luminescence in blue, green, yellow, orange, or red colors, depending on factors such as morphology, doping, temperature, excitation wavelengths, and the synthesis method. This variation in luminescence is attributed to the presence of various defects, including oxygen antisites, zinc vacancies, complex defect structures, zinc interstitials, and surface-related defects[51,52]. These defects create energy levels within the band gap, allowing radiative recombination of electrons and holes, resulting in visible green emission[20].

Figure 6 presents an AFM image of a thin film containing 1 wt% ZnOnps dispersed in a PVA matrix. Figure 6(a) displayed the two-dimensional

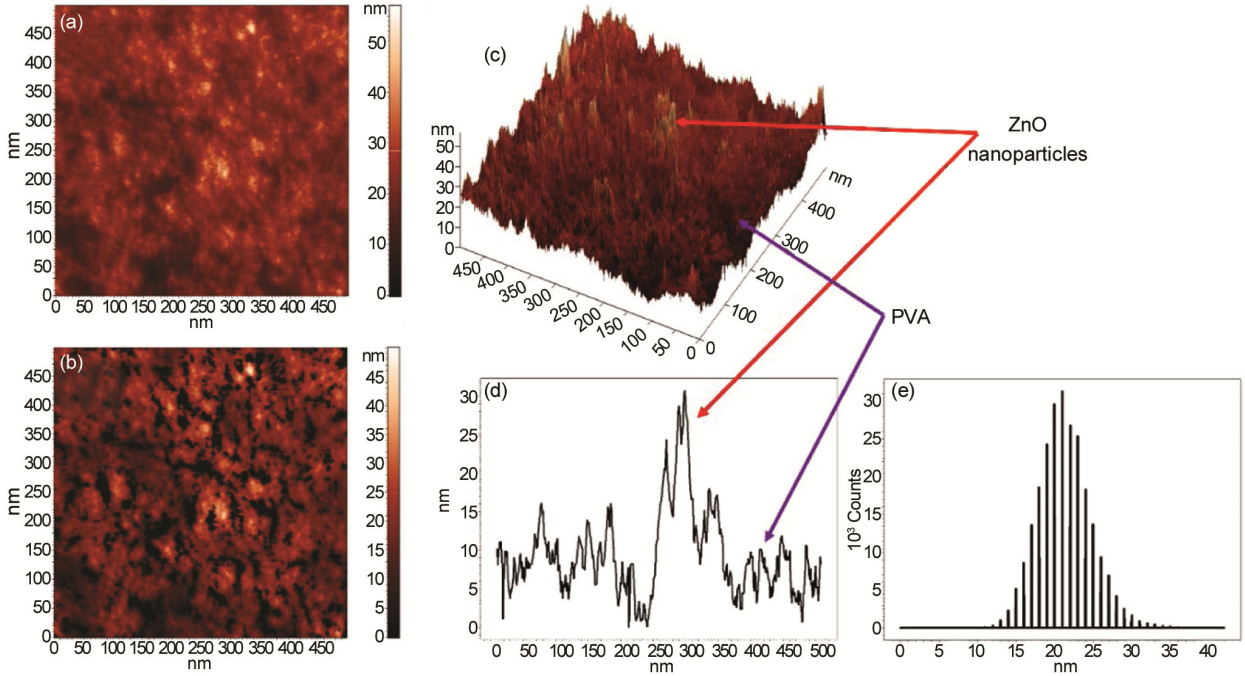

Fig. 7 — (a-e) shows the two-dimensional topographical map, grain size analysis, three-dimensional view, the average height profile and a histogram for particle size vs count receptively for a thin film of 5 wt% ZnOnps in PVA matrix deposited on a Si substrate

topographical map, while Fig. 6(b) gave grains analysis, Fig. 6(c) provided a three-dimensional view, Fig. 6(d) the average height profile (graph shows the variation in height across the sample surface) andFig. 6 (e) gave histogram of the histogram for particle counts vs size of the 1 wt% nanocomposite film, all within a scan area of 500 × 500 nm². From the topographical observation, it can be seen that bright zones corresponded to ZnOnps, with height ranging up to 40 nm, and dark zones at comparatively lower heights corresponded to the PVA matrix. Grain analysis indicated elongated domains with dispersion of nanoparticles in the PVA matrix, which ensures uniform dispersion of ZnOnps in the PVA matrix[53-55]. However, minor height fluctuations and irregular grain boundaries may also indicate local structural defects or inhomogeneities in the film, possibly arising from nanoparticle-polymer interactions.A three-dimensional view of the deposited composite film indicated mountains due to ZnOnps, these appeared as sharp peaks in an average height profile plot. The planer surface in three-dimensional view was due to the presence of a PVA matrix, it appeared as lower peaks in Fig. 6(d). The interconnection of Fig. 6(c-d) is explained by indicating with arrows for better clarity[56-60]. The histogram indicated particle size vs count ranges between 10 nm to 40nm with a peak at around 25nm.

Figure 7(a-e) indicated similar images of a two-dimensional view, grain analysis view, average height profile, three-dimensional view, and histogram size vs count of 5 wt% ZnOnps in the PVA matrix. The Root Mean Square (RMS) roughness of 3.471 nm and the roughness average (Ra) of 2.717 nm at 1 wt% ZnO increase to an RMS roughness of 5.049 nm and a Roughness Average of 3.932 nm at 5 wt% ZnO, according to the statistical parameters obtained from AFM analysis. It can be seen that brighter zones in Fig. 7(a) had increased as compared to Fig. 6(a), this was caused by the elevated concentration of ZnOnps within the nanocomposite films, surface roughness increased due to the higher concentration of nanoparticles, leading to more prominent height variations up to 55nm (on the color bar). Grain analysis indicated enhanced elongated domains with dispersion of 5 wt% nanoparticles in the PVA matrix, which can alter the mechanical strength of the film. In a three-dimensional view mountain indicating the presence of ZnOnps exhibited more pronounced surface features, depending on the nanoparticle distribution. Histogram for 5 wt% ZnOnps in PVA matrix indicated particle size vs count ranges between 10 nm to 35nm with peak for maximum count at ~25nm. It can be seen that the surface of the films was nearly smooth, confirming good dispersion of ZnOnps. The average height profile consisted of

peaks at a certain level, ensuring that there was no agglomeration of nps. Similar atomic force microscopy images are reported by Chauhan *et al.*[61] they deposited films of PVA/ZnO composite by Impregnation of ZnO Nanoparticles into the PVA Matrix. They showed a height profile in the micrometre range due to agglomeration of ZnO nanoparticles, while uniform films have been obtained by using the solution casting method at low concentrations of ZnOnps in the polymer matrix.

4 Conclusion

This research explored polyvinyl alcohol (PVA) and zinc oxide (ZnO) nanoparticle-based nano composite thin films prepared by solution casting technique, highlighting their tunable optical and structural properties. By varying ZnO concentration, the study showed a shift in the optical band gap, with UV-Visible spectra revealing absorption peaks at 370 nm and 379 nm for PVA-ZnO composites. X-ray diffraction confirmed improved crystallinity, and AFM ensured uniform nanoparticle dispersion. Photoluminescence spectroscopy indicated strong emission at 371 nm, corresponding to near-band-edge transitions. These findings highlight the potential of PVA/ZnO nanocomposites for optoelectronic devices like UV detectors, LEDs, and sensors. Future work will focus on studying their electrical conductivity, optimizing nanoparticle surface functionalization, assessing long-term stability, and exploring integration into flexible substrates. Extending this approach to other polymer–nanoparticle systems could also enable multifunctional materials for various optical and electronic applications.

References

1 Martin M, Prasad N, Sivalingam M M, Sastikumar D & Karthikeyan B, *J Mater Sci Mater Electron,* 29 (2018) 365, https://doi.org/10.1007/s10854-017-7925-z.

2 Pawar S P, Biswas S, Kar G P & Bose S, *Polymer,*84 (2016) 398, doi: 10.1016/j. polymer.2016.01.010.

3 Saini I, Sharma A, Dhiman R, Aggarwal S, Ram S & Sharma PK, *J Alloys Compd,* 714 (2017) 172, doi: 10.1016/j.jallcom.2017.04.183.

4 Abdullah ZW, Dong Y, Davies I J & Barbhuiya S, *Polym Plast Technol Eng,* 56 (2017) 1307, doi: 10.1080/03602 559.2016.1275684.

5 Ambrosio RC, Carrillo AC, Mota ML, Torre K, Torrealba R, Moreno M, Vazquez H, Flores J & Vivaldo I, *Polymers,* 10 (2018) 1370, doi.org/10.3390/polym 10121370.

6 Zhong Y, Lin Q, Yu H, Shao L, Cui X, Pang Q, Zhu Y & Hou R, *Front Chem,* 12 (2024) 01, doi:10.3389/ fchem.2024.1376799.

7 Ibrahim A M, Nasr GM, Ahmed RM &Kelany N A, *Sci Rep,* 14 (2024) 5391, doi: 10.1038/s41598-024-55818-8.

8 Limpan N, Prodpran T, Benjakul S & Prasarpran S, *Food hydrocolloids*, 29 (2012) 226, doi: 10.1016/j.foodhyd. 2012.03.007.

9 Kaur R, Bhullar G K & Raina KK, *J MolLiq,* 294 (2019) 111664, doi: 10.1016/j.molliq.2019.111664.

10 Chastellain M, Petri A & Hofmann H, *J Colloid Interface Sci,* 278(2004) 353, doi: 10.1016/j.jcis.2004.06.025.

11 Lee J, Easteal A, Pal U & Bhattacharyya D, *Current Appl Phys,*9 (2009) 792,doi: 10.1016/j.cap.2008.07.018.

12 Kang Y, Yu F, Zhang L, Wang W, Chen L & Li Y, *Solid State Ion,* 360(2021) 115544, doi: 10.1016/j.ssi.2020.115544.

13 Uribe-Lopez M C, Hidalgo-Lopez M C, Lopez-Gonzalez R, Frias-Marquez D M, Nunez-Nogueira G, Hernandez-Castillo D & Alvarez-Lemus M A, *J Photo chem Photo biol A,* 404 (2021) 112866. doi:10.1016/j. jphotochem.2020.112866.

14 Lamia Z, *Mater Sci Engg: B*, 174 (1-3) (2010) 18,doi: 10.1016/j.mseb.2010.07.001.

15 Moszak K, Szczurek A, Babiarczuk B, Borak B & Krzak J, *Adv Mater Lett,* 8 (2017) 542, doi:10.5185/AMLETT. 2017.7108.

16 Dang Z M, Yuan J K, Yao S H & Liao R J, *Adv Mater,* 25 (2013) 6334, doi: 10.1002/adma.201301752.

17 Khan S A, Rhman A, Babiker F & Ibrahim D A, *Mater Res Express*, 8 (2021) 075002, doi:10.1088/2053-1591/abf081.

18 Nayak S M, Anjum R, Husain J, Dattu H, Afrooze A & Rahika G, *Ferroelectrics,* 577 (2021) 221.

19 Sugumaran S, Bellan C S & Nadimuthu M, *Int J Polym Anal Charact,* 19 (2014) 549.

20 Guedri A, Boudine B, Hafdallah A & Zaabat M, *J Inorg Organomet P Mater,* 30 (12)(2020) 4884, https://doi.org/10. 1007/s10904-020-01604-8.

21 Bhullar G K & Raina KK, *AIP Conf Proc,* 24 1591 (1) (2014) 972, https://doi.org/10.1063/1.4872822.

22 Wen Y-H, Tsou C-H, Huang D, Yu Y-Q, Zhu H, Du J, Wang Z-H, Gao C, Zhang X-M, De Guzman M R & Zheng Y-T, *Polym Bull,* 79 (6) (2021) 3847, https://doi.org/10.1007/ s00289-021-03666-1.

23 Ai L, Wang Y, Tao G, Zhao P, Umar A, Wang & He H, *Molecules, 24* (2019) 503, https://doi.org/10.3390/ molecules 24030503.

24 Xie W-Q, Yu K-X & Gong Y-X, *Cellulose,* 26 (4) (2019) 2363, https://doi.org/10.1007/s10570-019-02245-y.

25 Meera K & Ramesan M, *J Thermoplast Compos Mate*, 37 (9) (2023) 3036, https://doi.org/10.1177/08927057231222833.

26 Abdeltwab E & Atta A, *Int J Modern Phys B,* 35 (30) (2021)2150310, https://doi.org/10.1142/s021797 922150 3100.

27 Kumar D, Vijayan N, Khanna P K, Banerjee S & Jat S K, *Int J Green Nanotechol*, 4 (3) (2012) 408, https://doi.org/ 10.1080/19430892.2012.738509.

28 Restrepo I, Mangalaraja R V, Flores P, Benito N, Rodriguez-Llamazares S & Medinam C, *Mater Res Exp,* 4 (10)(2017) 105019, https://doi.org/10.1088/2053-1591/aa8b8d.

29 Premkumar H, *Nano-Struct Nano-Objects,* 39 (2024) 101208, doi: 10.1016/j.nanoso. 2024.101208.

30 Kumar R & Raina K K, *LiqCryst,* 42 (1) (2015) 18.

31 Rahman M, Hossain J, Kuddus A, Tabassum S, Humaun M H K, Rubel K, Shirai H, Bakar A & Ismail M, *Appl Phys A,* 126 (2020) 145, doi:10.1007/s00339-020-3331-0.

32 Asadpour S, Raeisivanani A, Kooravand M & Asfaram A, *J Cleaner Prod* 362 (2022) 132297, doi: 10.1016/ j.jclepro.2022.132297.

33 Fernandes D M, Hechenleitner A A W, Lima SM, Andrade LHC, Caires A R L & Pineda E A, *Mater Chem Phys,* 128 (2011) 371, doi: 10.1016/j.matchemphys.2011.03.002.

34 Mei H, Piccardo P, Carraro G, Smerieri M & Spotorno R, *J Energy Storage,* 72 (2023) 108244, doi: 10.1016/ j.est.2023.108244.

35 Kaur R, Kaur N, Bhullar G K, Advances in Fabrication Techniques for Hybrid Nanomaterials. In: Khanna V, Mahajan P, Sharma P, editors. Innovations and Applications of Hybrid Nanomaterials. New York (NY): IGI Global Publisher; (2024) 16, doi: 10.4018/979-8-3693-3268-9.ch002.

36 R Kaur R, Bhullar GK & Raina KK, *Liq Cryst* 43 (2016) 1760, doi: 10.1080/02678292.2016.1200687.

37 R Kaur R, Bhullar G K & Raina KK, *Liq Cryst,* 39 (2012) 1375, doi:10.1080/02678292.2012.717113.

38 Suchea M, Christoulakis S, Katsarakis N, Kitsopoulos T & Kiriakidis G, *Thin Solid Films,* 515 (2007) 6562, https://doi.org/10.1016/j.tsf.2006.11.151.

39 Beyazay E, Sahin N, Karabul Y, Kilic M & Ozdemir Z G, *J Appl Polym Sci,* 140 (2023) 1, doi:10.1002/app.54640.

40 Yadav P, Lahariya V N, Pandey P P, Behl S & Raghav R, *J Mater Sci Mater Electron,* 34 (2023)787, doi:10.1007/s 10854-023-10178-3.

41 Roy A S, Gupta S, Sindhu S, Parveen A & Ramamurthy PC, *Composites, Part B Engineering,* 47 (2013) 314, doi: 10.1016/j.compositesb.2012.10.029

42 Makuła P, Pacia M & Macyk W, *J Phys Chem Lett* 9 (2018) 6814, doi: 10.1021/acs.jpclett.8b02892.

43 Zhong H, Pan F, Yue S, Qin C, Hadjiev VG, Tian F, Liu X, Lin F, Wang Z & Bao J, *J Phys Chem Lett,* 14 (2023) 6702, doi: 10.1021/acs.jpclett.3c01416.

44 Sathish S, Shekar B C, Kannan S C, Sengodan R, Dinesh KPB & Ranjith kumar R, *Int J Polym Anal Charact* 20 (2014) 29, doi: 10.1080/1023666X.2015.975414.

45 Agarwal S, Saraswat Y K & Saraswat V K, *Open Phys J,* 3(2016) 63, doi: 10.2174/1874843001603010063.

46 Mathen J J, Madhavan J, Thomas A, Edakkara A J, Sebastian J & Joseph G P. *J Mater Sci Mater Electron* 28 (2017) 7190, doi:10.1007/s10854-017-6400-1.

47 Khan S A, Zain Z M, Mansoor M, Hasan Mahfuz M M, Rahman A, Rashid MAN & Rais M S, Materials Today: Proceedings 47(2021) 2615, doi: 10.1016/j.matpr.2021. 05.197.

48 Khan S A, Rahman A, Khan W & Haider S M, *J Mech Sci Technol,* 37(2023) 1, doi:10.1007/s12206-022-0806-2.

49 Jangir L K, Kumari Y, Kumar A, Kumar M & Awasthi K, *Mater Chem Front,* 7 (2017) 730, doi:10.1039 /C7QM00058H.

50 Ristic M, Music M S, Ivanda M & Popovic S, *J Alloys Compd* 397 (2005) 1, doi: 10.1016/j.jallcom.2005 .01. 045.

51 Poornima N, Vimalkumar T V, Rajeshmon V G & Kartha C S & Vijay Kumar KP, *Int J Photoenergy,* 2013 (2013)105796, doi:10.1155/2013/105796.

52 Dijken AV, Meulenkamp E A, Vanmaekel bergh D, Meijerink A, *J Phys Chem B* 104 (2000) 1715, doi:10.1021/jp993327z.

53 Kaur S, Kaur R & Gupta S, *Phys Scr,* 99 (2024) 115993, https://doi.org/10.1088/1402-4896/ad868a.

54 Kumar R, Kaur R & Raina K K, 133 (2025), https://doi.org/10.1007/978-981-96-3821-5_7.

55 Bhullar G K, Kaur R, Kumar R & Raina K K, Liq Cryst, (2025)1, doi.:10.1080/02678292.2025.2515126.

56 Joshua A M, Cheng G & Lau E V, *Appl Surf Sci Adv,* 17(2023) 100448, doi: 10.1016/j.apsadv.2023.100448.

57 Bhullar G K, Kaur R & Raina K K, *J Electron Mater,* 44 (2015) 3422, doi: 10.1007/s11664015-38684.

58 Bhullar G K, Kaur R & Raina K K, *J Appl Polym Sci,* 135(2015) 1, https://doi.org/10.1002/app.41386.

59 Bhullar G K, Kaur R & Raina K K, *Thin Solid Films,* 782 (2023) 140023, doi.org/10.1016/j.tsf.2023.140023.

60 Bhullar G K, Kaur R & Raina K K, *AIP Conf Proc,* 1536 (2013) 491, doi:10.1063/1.4810315.

61 Chouhan S, Bhatt R, Bajpai A K, Bajpai J & Katare R, *Fiber Polym,* 6 (2015) 1243, doi: 10.1007/s12221-015-1243-y.